Materials Advances

ROYAL SOCIETY OF CHEMISTRY

PAPER

View Article Online
View Journal | View Issue

Cite this: *Mater. Adv.*, 2026, 7, 4837

Tunable optical responses in cyanoester-based organic π-conjugates for selective sensing of aliphatic diamine vapors

Akshita Jain, Syed Noushin, Pralok K. Samanta and Manab Chakravarty *

Amine addition to α,β-unsaturated cyanoesters generally favors the competitive 1,4-addition over the 1,2-addition/elimination (nucleophilic acyl substitution). This work describes an easy, metal-free synthesis of a cyanoester-functionalized, conformationally twisted π-conjugate, **CYE**, which exhibits aggregation-induced emission (AIE) and decent solid-state emission. Such molecules exhibit visually detectable responses against diamine vapors. More importantly, vapor-induced fluorochromism at the solid–vapor interface was selective to the specific alkyl chain length, highlighting their sensitivity to subtle structural variations. Notably, the fluorophores show diverse, concentration-dependent fluorescence responses toward selective aliphatic biogenic amines (BAs) in the solid–vapor phase. Gradual exposure of the fluorophore to BA vapors induces a visible color change from orange through yellow to green, accompanied by an enhanced quantum yield. Mechanistic investigations reveal the gradual formation of mono- and diamides from the reactions between **CYE** and putrescine (PUT). The acid analog **CYA** formed a salt by reacting with ethylenediamine (EDA). Furthermore, these fluorophore-coated platforms are used for practical applications to monitor the freshness of Indian cottage cheese (paneer), during which significant fluorescence quenching was observed. These findings highlight the potential of **CYE** and **CYA** fluorophores as an efficient platform for detecting BAs and monitoring food quality.

Received 11th February 2026,
Accepted 4th April 2026

DOI: 10.1039/d6ma00194g

rsc.li/materials-advances

Introduction

The 1,2-addition/elimination (nucleophilic acyl substitution) of an amine to α,β-unsaturated esters is a well-documented process that historically forms the most stable amide molecules. This fundamental event has been utilized for various synthetic and biological evaluations.[1–4] Furthermore, diamine reactions with cyano esters became essential for the development of dimeric tyrphostins (Fig. 1a), which exhibit anticancer activity.[5,6] Notably, well-decorated fluorophores with cyanoester functionality can detect the vital analyte, the cyanide anion (Fig. 1b), exhibiting a color change in both the solution and solid states *via* a Michael-type (1,4) addition.[7,8]

It is highly pertinent to note that the reaction between an amine nucleophile and α,β-unsaturated cyanoesters primarily progresses through an aza-Michael addition reaction.[9] However, aminolysis of the ester, forming an amide, is also a competing side reaction for the primary amine nucleophile. Thus, individual 1,2- and 1,4-addition of amines is common, but there is hardly any investigation into competitive 1,2- and 1,4-addition reactions of cyanoester conjugates. Our detailed literature survey reveals a relevant reaction where thiourea reacts with an unsaturated cyanoester, leading to the formation of a heterocycle (Fig. 1c).[9]

These reactions motivated us to design a new class of α,β-unsaturated cyanoester probes that display both solution- and solid-state emissions and are utilized to detect diamines, especially biogenic amines (BAs). In our recent research on finding suitable probes for BAs,[10–13] cyanoacid has been proven to be a potential platform for concentration-tuned detection of putrescine (PUT) and cadaverine (CAD), and has been realized as a promising platform for monitoring food freshness. However, emissive cyanoesters, a reactive platform for amines *via* both 1,2- and 1,4-additions, have not been evaluated for the detection of BAs so far. Of note, BAs are primarily formed through microbial decarboxylation of amino acids and found in fermented food and beverages. It is also produced during the spoilage of protein-rich foods (such as fish meat and paneer).[14–18] Some of these are highly toxic and harmful to flora and fauna when their concentrations exceed 20 mg kg^{-1}. Therefore, rapid and sensitive detection of such BAs is crucial. There are various expensive, time-consuming mass spectrometric methods for their detection. Moreover, these techniques require specialized expertise and a well-equipped laboratory for

Department of Chemistry, Birla Institute of Technology and Sciences-Pilani, Hyderabad Campus, Jawaharnagar, Medak, Shamirpet, Hyderabad, 500078, India. E-mail: manab@hyderabad.bits-pilani.ac.in

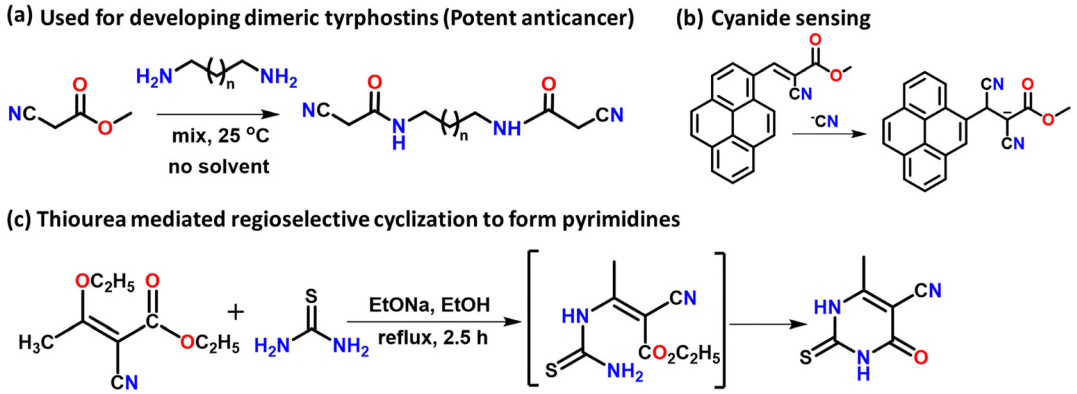

Fig. 1 Reported cyanoesters reacting with (a) diamines, (b) cyanide, and (c) thiourea.

their effective implementation.[19–23] In this context, many optical sensors offer alternative strategies[24–26] but still face numerous challenges, including poor colour contrast, lack of reusability, and relatively lower selectivity/sensitivity.

Highly sensitive, well-recognized fluorescent dyes are primarily effective in the solution state, rather than in the solid state, which creates a barrier for on-site applications. Furthermore, concentration-dependent detection of BAs is crucial for reducing food waste; however, only a few probes can detect them in the vapor phase.[27–29] Herein, we report a metal/ligand-free access to a cyanoester-linked anthracene-based fluorophore, **CYE**, which emits in solution, aggregates, and the solid state. The decent emission in the solid state is used to detect mainly aliphatic BAs, such as ethylenediamine (EDA), 1,3-diaminopropane (DAP), and PUT (a crucial BA indicating food freshness), with high sensitivity and color contrast. Notably, both EDA and DAP are industrially and pharmaceutically important diamines that exhibit potential toxicity to the animal kingdom and contribute to environmental pollution when reaching a specific threshold. Interestingly, unlike other systems, this probe is most useful in the solid state, rather than in solution. Thus, it has proven to be a valuable platform for real-world applications. One crucial point to note is that diamines with shorter spacer lengths, up to four CH_2 units, induce a better fluorescence response compared to those with longer chains, such as 1,5-diaminopentane (1,5-DAP) and 1,6-diaminohexane (1,6-DAH), following the order EDA ≈ 1,3-DAP ≈ 1,4-DAB > 1,5-DAP > 1,6-DAH. Moreover, the diamine reacts gradually with the cyanoesters, and the product formation varies with the diamine concentration; a corresponding color change is visible to the naked eye. The experimental and theoretical studies elucidate the variations in the outcomes. We used these dyes to assess the freshness of Indian cottage cheese and to validate the on-site application.

Results and discussion

Design and synthesis of simple and suitable molecular probes

When designing an appropriate molecule, the following factors were considered: (a) achieving strong emission in solution by incorporating extensive π-conjugation with the renowned fluorescent building block anthracene, (b) enabling aggregate/solid-state emission by joining a small flanking donor, like a dimethoxy group, along with a substituted vinyl stator to introduce conformational twists that prevent strong intermolecular π···π stacking and become emissive due to restricted intramolecular motion in the aggregate/solid state, and (c) creating a reactive site for amine attack, as commonly reported in the literature.[30–32] Detection of diamines is achieved through the gradual 1,2-nucleophilic addition/elimination of two $-NH_2$ groups to an ester group, forming a diamide and shifting the probe's emission profile. The inclusion of an acrylic cyano group promotes inter- and intramolecular interactions between the cyano and unreacted $-NH_2$ groups of diamines.[33]

The target molecule was efficiently synthesized *via* a simple and economical route. Dimethoxy-linked anthracenyl phosphonate was introduced using a previously established Friedel–Crafts-type arylation reaction.[34] The methoxy group acts as an electron-donating auxochrome that can improve the molar extinction coefficient and fluorescence properties by promoting the electron push–pull effect within the molecular structure. Furthermore, the methoxy groups introduce steric factors and multiple tunable noncovalent interactions, providing an excellent emissive platform with a stable structure in the solid state.

The same phosphonate, after a controlled partial olefination reaction with terephthaldehyde, yielded **DAA** in 49% purity, and the unreacted phosphonate was successfully recovered. Subsequently, **DAA** was converted into the desired compound **CYE** in 64% yield (diastereomeric ratio, dr: 60 : 40) *via* a Knoevenagel reaction, serving as ideal reactive centres for 1,2-nucleophilic addition/elimination (Scheme 1). The compound is soluble in most organic solvents and well characterized by ^1H and ^{13}C NMR and HR-MS.

Photophysical studies of CYE probes

These probes (10 μM) exhibit absorption maxima (λ_{abs}) in the range of 340–399 nm due to π–π* transition in almost all types of solvents tested herein. The emission maxima (λ_{em}) at ~550 nm with ~8–12% relative quantum yield (Φ_f) were primarily observed in nonpolar solvents, and very weak

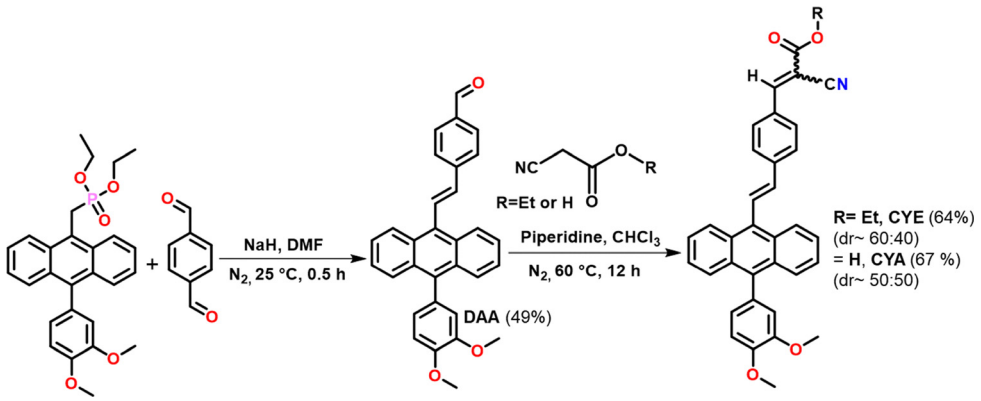

Scheme 1 Synthesis of diastereomeric fluorophores **CYE** and **CYA**.

emission (1–2% Φ_f) was noticed at a λ_{em} of 610–630 nm in polar solvents. Thus, the weakly intense dye exhibits solvatochromism (Fig. S1 and Table S1), indicating strong intramolecular charge transfer within the system, which is further supported by a density functional theory (DFT) study at the CAM-B3LYP/6-31G(d) level of theory (Fig. S2). The highest occupied molecular orbital (HOMO) is mainly localized on the electron-rich anthracene unit. In contrast, the lowest unoccupied molecular orbital (LUMO) is localized mainly on the electron-deficient cyanoester part. Thus, a fairly well-separated HOMO and LUMO, which would facilitate efficient charge transfer and, therefore, the emission intensity, is not promising.

As established earlier,[35] such molecular twists would likely favour potential aggregation-induced emission (AIE) behaviour in a **CYE** molecule. Therefore, AIE studies were performed by gradually increasing the water fraction [f_w (v/v%)] in 10 μM probe solutions in acetonitrile, which exhibited a prominent AIE effect (Fig. 2, Fig. S3 and Table S2) with red-shifted emission, representing the formation of J-type aggregates, a characteristic feature of the AIE phenomenon.[36] The aggregation corresponding to the highest fluorescence intensity is supported by dynamic light scattering (DLS) measurements, which reveal an average particle size of 5.5 nm for **CYE** (Fig. S3).

This AIE feature confirms the emission in the solid state. Thus, we focus on the solid-state photophysical properties, which exhibit an absorption maximum at 470 nm. The corresponding emission maximum occurs at ~601 nm, with a measurable, visually detectable absolute Φ_f of 8.09%, suggesting its potential applicability in solid-state chemosensing (Fig. S4).

Fluorescence response influenced by various amines in solution and the AIE state

A 10 μM dioxane solution of **CYE** (reddish orange) was treated with numerous amine solutions at very high concentrations (100 μM in dioxane), since solution-state detection is insignificant, as observed in our previous studies.[12] Various amines, including EDA, 1,3-DAP, PUT, 1,5-diaminopentane (1,5-DAP or CAD), 1,6-diaminohexane (1,6-DAH), 2-phenylethylamine (2-PEA), ammonia, triethylamine (Et_3N), aniline, *n*-butylamine, diisopropylethylamine (DIPEA), tryptamine, spermine, and spermidine (Fig. 3 and Fig. S5), were screened for this study. Furthermore, a decently emissive AIE state of the **CYE** molecule (99% water in acetonitrile) was also treated with the amine solution. Unfortunately, no significant responses were detected in either the solution or the AIE state (Fig. 3 and Fig. S5). This implies that these amines do not immediately react with

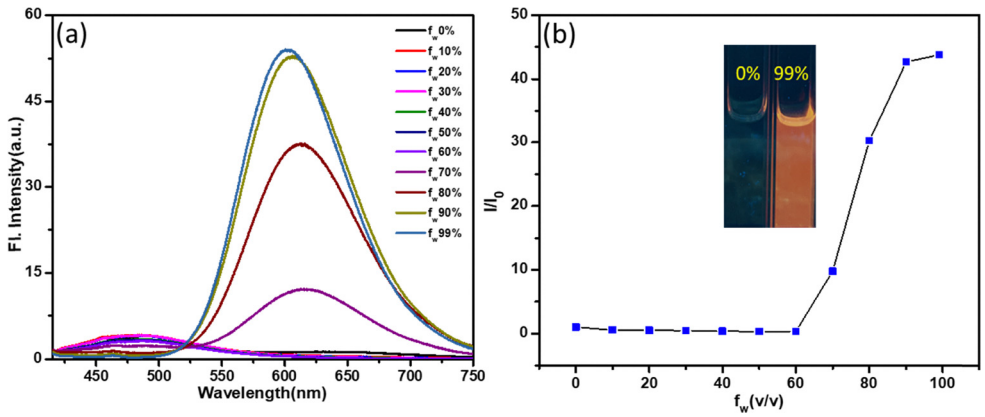

Fig. 2 AIE study: (a) emission spectra and (b) I/I_0 plot of **CYE** with gradual increase of water fraction in a 10 μM probe solution in acetonitrile. λ_{ex} = 398 nm.

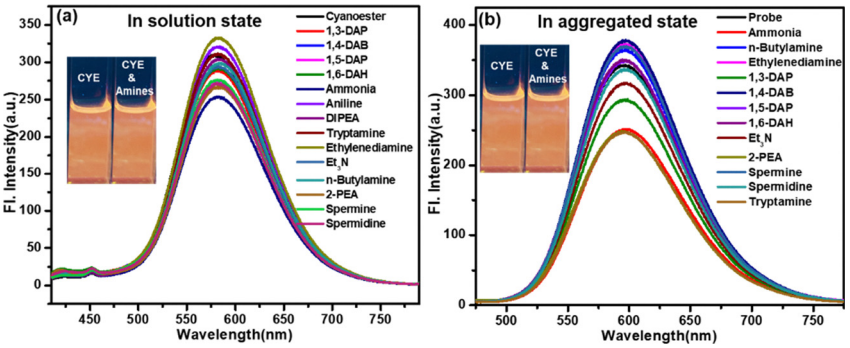

Fig. 3 Emission spectra of **CYE** in (a) the solution state (10 μM in dioxane) and (b) the aggregated state after the addition of amines (100 μM in DMAc). (λ_{ex} = 398 nm).

cyanoester functional groups in solution, as evidenced by the observed changes in the emission spectra. A strong electron-poor environment around such fluorophores may hinder the approach of amines to the reactive carbonyl group, reducing the effective collision rate (due to several solute–solvent interactions) required to initiate the addition reaction. In contrast, the controlled molecular motion in the solid state can facilitate selective interaction with the amine vapor at the carbonyl centers, leading to a change in emission.

Photophysical features in the solid state and response to BA vapors

Due to failures in solution/aggregate states, we shifted to solid-state platforms. Therefore, a thin film was prepared on a coverslip by drop-casting 30 μL of 0.01 M **CYE** in 1,4-dioxane, followed by evaporation at room temperature, resulting in a visually detectable, reddish-orange-emitting platform. These drop-cast coverslips were then exposed to 30 μL of liquid amine for 20 minutes (response time) inside a sealed 200 mL jar under identical conditions.

Upon exposure to amine vapors, the thin film, which emitted reddish-orange light, changed to a yellow- or green-emitting platform. Hence, systematic studies were performed using these emissive platforms by exposing them to amine fumes and recording their emission profiles. **CYE** displayed a notable response to selected diamines, including EDA, 1,3-DAP, and 1,4-DAB, with a blue shift of 84–90 nm, resulting in a change from orange to green emission. A comparatively weaker response was detected for 1,5-DAP and *n*-butylamine, where the blue shift range is only 14–50 nm, leading to a yellow-emitting platform. No response was observed with other amines, including 1,6-DAH, spermine, spermidine, ammonia, Et_3N, and 2-PEA (Fig. 4 and Fig. S6 and Table 1). Notably, the primary amine, *i.e.*, *n*-butylamine, was also somewhat responsive, but the effect was not significant, with a wavelength shift of only 51 nm. Furthermore, food spoilage systems may produce many other potential interfering substances, such as organic acids (acetic acid/lactic acid), alcohols (ethanol), and aldehydes (acetaldehyde/benzaldehyde). Upon treating all these substances under similar experimental conditions, no significant responses were observed in either the solid or solution state (Fig. S7), indicating that **CYE** selectively detects amines associated with food spoilage. The lower nucleophilicity of these interfering substances was insufficient to demonstrate any changes in emission profiles.

Concentration-induced change in emissions

Furthermore, the same **CYE** platform was tested for the potential concentration-tuned emission ability with the most

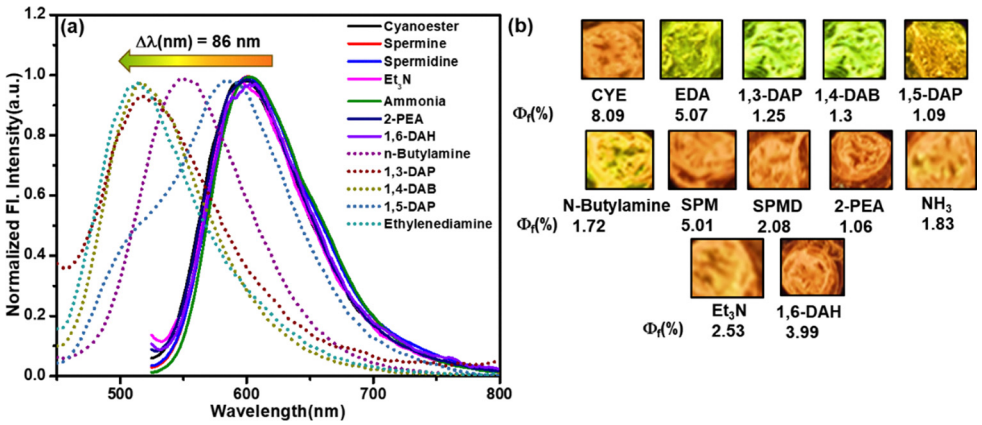

Fig. 4 (a) Solid-state emission profile of **CYE** before and after exposure to amine vapors; (b) the images of coverslips taken under a 365 nm UV lamp for **CYE**. λ_{ex} = 450 and 525 nm.

Table 1 Details of the solid-state emission profile of **CYE** with various amines (λ_{ex} = 398 nm)

	Cyanoester			
Amines	λ_{em} (nm)	$\Delta\lambda$ (nm)	Φ_f (%)	Concentration (mg L^{-1})
Probe	601	—	8.09	—
1,3-DAP	515	86	1.25	133.2
1,4-DAB (PUT)	517	84	1.30	131.55
1,5-DAP (CAD)	585	16	1.09	130.5
1,6-DAH	601	0	3.99	126
Ethylenediamine	511	90	5.07	135
Spermidine	601	0	2.08	138.7
Spermine	601	0	5.01	140.5
n-Butylamine	550	51	1.72	111
Ammonia	601	0	1.83	109.5
Triethylamine	601	0	2.53	108.9
PEA	601	0	1.06	144.6

vital BA, *i.e.*, PUT (one of the food freshness detectors), because it displayed a substantial shift from reddish orange to green (84 nm shift) in the solid platform. The platform was exposed to PUT vapors for 20 minutes at 25 °C in a closed jar (200 mL) containing a gradually increasing concentration of PUT liquid. The reddish orange emissive platform remained unchanged up to 5 μL (21.9 mg L^{-1}) of PUT, but the change began from 10 μL (43.8 mg L^{-1}) and formed a yellow emissive platform [557 nm, 39 nm blue shift, Φ_f (%) = 4.21] in 15 μL (65.7 mg L^{-1}) of PUT. Further increases in concentration (87.7 mg L^{-1}, 20 μL) resulted in the yellow coverslip turning completely green (532 nm, Φ_f (%) = 5.19, 65 nm blue shift). However, we examined up to 40 μL (175.4 mg L^{-1}) of PUT, but the overall change was limited to the green emission (517 nm, 79 nm blue shift), with a marginal increase in Φ_f (%) to 6.21. Thus, we observed a significant shift in emission from red to green, with an intermediate yellow platform, which was analyzed to determine the origin of this transition. After the reaction between the ester and the amine, the electronic conjugations in the amide are significantly reduced, leading to a blue-shifted emission (Fig. 5 and Fig. S8). Two excitation wavelengths (440 and 480 nm) were selected based on the distinct absorbance maxima of the system. The absorbance band at 470 nm corresponds to the native **CYE** fluorophore, whereas the band at 431 nm appears after interaction with putrescine (PUT), indicating the formation of the responsive species (Fig. S8).

A comparative study with acid analogs

In our earlier studies, we demonstrated that a cyanoacid emitter is an excellent platform for detecting PUT and CAD.[11] In this regard, we herein plan to compare our observed results using the ester dye **CYE** with the analogous acid **CYA** (Scheme 1). The solid-state emission, with a λ_{max} at 618 nm and Φ_f (%) = 13, was noted for the dye **CYA**. Various amine vapors were exposed in a manner to **CYE**, and the result was quite unexpected because only two amine vapors (*n*-Bu-NH_2 and EDA) showed an apparent change in emission from red to yellow (550–560 nm), showing a blue shift of 40–50 nm (Fig. S9 and Table S3). Although such a blue shift is reasonable and attributed to the lack of conjugation after forming a salt, the reason behind this selectivity towards only these two amine vapors is subject to further investigation.

Mechanistic insights

In the case of **CYE**, the diamine response was consistent with increasing chain length, in the order EDA > 1,3-DAP > 1,4-DAB > 1,5-DAP > 1,6-DAH. The hydrophilic diamine with a shorter spacer is more beneficial than a relatively more hydrophobic diamine possessing a long alkyl chain (–CH_2) spacer. The differences in fluorescence response can be attributed to two main factors. Firstly, short-alkyl-chain hydrophilic diamines, such as EDA, slowly undergo 1,2-addition to the two ester functionalities of the **CYE** probe, accompanied by hydrogen-bonding interactions with the cyano group. This facilitates the gradual formation of cyano-diamide adducts (*vide infra*). Secondly, the vapor pressure of these diamines significantly influences their diffusion and interactions at the solid–vapor interface. At 20 °C, the vapor pressures follow the order: EDA (10 mmHg), 1,3-DAP (7.5 mmHg), 1,4-DAB (2.6 mmHg), 1,5-DAP

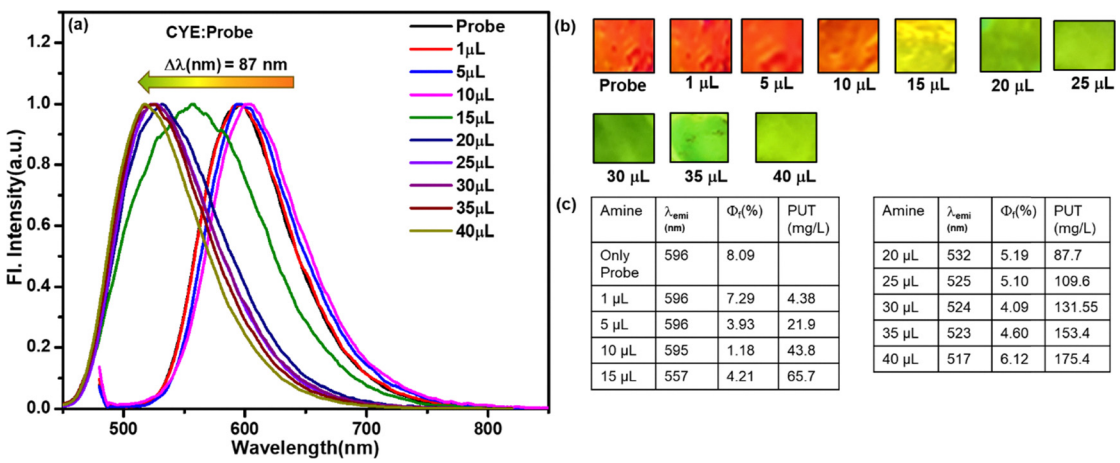

Amine	λ_{emi} (nm)	Φ_f(%)	PUT (mg/L)
Only Probe	596	8.09	
1 μL	596	7.29	4.38
5 μL	596	3.93	21.9
10 μL	595	1.18	43.8
15 μL	557	4.21	65.7

Amine	λ_{emi} (nm)	Φ_f(%)	PUT (mg/L)
20 μL	532	5.19	87.7
25 μL	525	5.10	109.6
30 μL	524	4.09	131.55
35 μL	523	4.60	153.4
40 μL	517	6.12	175.4

Fig. 5 (a) Emission spectra, (b) the images of the thin film upon exposure to different amounts of PUT for 20 min, and (c) the emission profile at different concentrations of PUT. λ_{ex} = 440 and 480 nm.

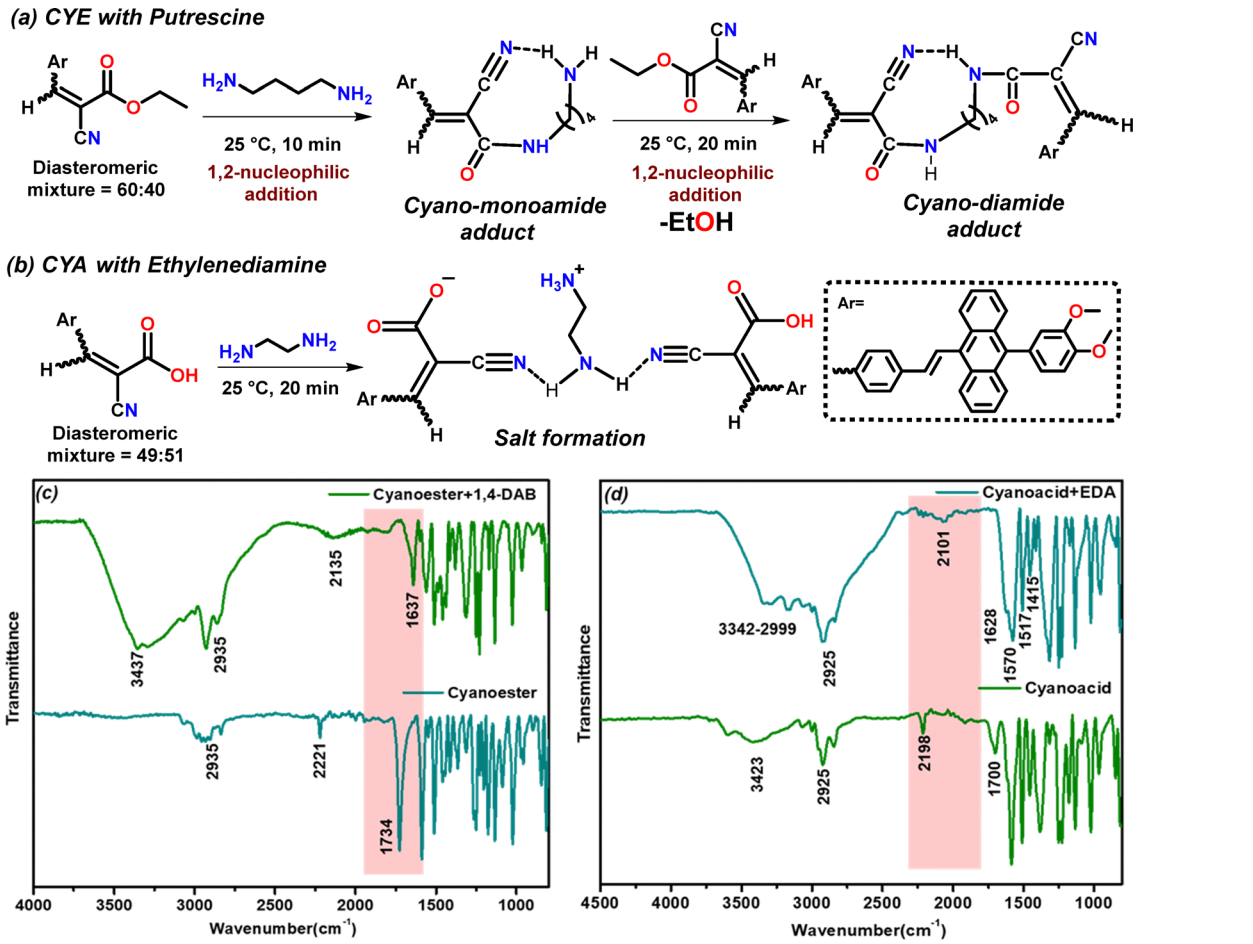

Fig. 6 Plausible mechanism for the reaction and interactions of (a) **CYE** and (b) **CYA** with diamines. FT-IR spectra of (c) **CYE** and 1,4-DAB-fumed **CYE** and (d) **CYA** and EDA-fumed **CYA**.

(1 mmHg), and 1,6-DAH (0.188 mmHg).[37–39] Therefore, the vapor pressure at room temperature correlates well with the observed fluorescence response. This result indicates that **CYE** is a good dye for wavelength shift. Detailed experimental studies were conducted to support this cyano-diamide formation (Fig. 6). Notably, cyanoamide formation was evidenced upon prolonged exposure of **CYE** to PUT vapors, as confirmed by FT-IR spectroscopy (Fig. 6c). A broad absorption band at 3437 cm^{-1}, corresponding to N–H stretching vibrations, emerged, which was absent in the pristine **CYE**, suggesting the formation of an amide. Concurrently, the intense C=O stretching band at 1734 cm^{-1} disappeared, with a new intense band appearing at 1637 cm^{-1}, further supporting the formation of an amide linkage. The IR absorption band at 2221 cm^{-1}, which confirms the presence of the C≡N group, gradually shifts by 86 cm^{-1} to 2135 cm^{-1}, indicating the reduced force constant of the –C≡N group because of its interactions with the amine functionality (Fig. 6c). In the case of **CYA**, ammonium carboxylate salt formation is recognized upon slow exposure of EDA vapor as observed from FT-IR studies (Fig. 6d) that depict a broad envelope at 3342–2999 cm^{-1} with the disappearance of the O–H stretching at 3423 cm^{-1} for pure **CYA**. Subsequently, respective signals (cm^{-1}) at 1628 and 1517 cm^{-1} indicate asymmetric and symmetric stretching of the $-NH_3^+$ unit.[40a] Moreover, the disappearance of intense C=O stretching at 1706 cm^{-1}, followed by the arrival of two bands at 1570 and 1415 cm^{-1}, further confirms the presence of asymmetric and symmetric stretching of the negatively charged carboxylate ion.[40b] The C≡N stretching at 2198 cm^{-1} is shifted to 2101 cm^{-1} due to the decrease of the force constant, arising from the ≡C–N···H interaction (Fig. 6d). The solid-state absorption spectra of **CYE** further validated such a ground state event, indicated by the shift of the absorption maximum of the reddish orange dye λ_{max} from 470 to 431 nm (yellow solid, 34 nm blue shift) upon exposure to PUT vapor (Fig. S10a). **CYA** displayed an absorption maximum at $\lambda_{max} \approx$ 465 nm, which shifted to 427 nm (a 38 nm blue shift; Fig. S10b). The blue shift is attributed to the strong electron-withdrawing ester group being replaced by the amide, which reduces electronic conjugation. This indicates that the changes in ambient light are also visually promising and easily detectable.

The yellow/green emissive solid compound formed after exposure to PUT and EDA vapors was scratched and dissolved in deuterated solvent for ^{1}H NMR and MeOH for LC–MS. The ^{1}H NMR spectrum shows the disappearance of signals at

approximately δ 4.4–4.3 and δ 1.3–1.2, corresponding to the O–CH_2–CH_3 moiety. Additionally, new peaks appear at δ 3.7 and δ 1.7–1.8, which can be attributed to CH_2 protons within the newly formed amide bond. As the sample was exposed to amine vapors, the vapor concentration could not be strictly controlled; hence, additional CH_2 signals indicate the presence of unreacted PUT at δ 2.7 and δ 1.7–1.8 (Fig. S11). These observations collectively support the occurrence of a carbonyl 1,2-addition/elimination of the amine to **CYE**, resulting in the formation of a cyano-diamide. LC–MS analysis reveals signals at *m*/*z* 582.4600 [CYE + PUT + H], indicating the formation of a cyano-monoamide species (Fig. S12). In contrast, the green-emissive compound showed a peak at *m*/*z* 1073.7100 [M–H], corresponding to the formation of a cyano-diamide derivative (Fig. S13). Similarly, the orange-emissive **CYA** transformed into a yellow-emissive solid, exhibiting a peak at *m*/*z* 572.2542 [M + H] in HR-MS, supporting the formation of a salt (Fig. S14).

The enhanced absolute quantum yields were elucidated by performing fluorescence (FL) lifetime decay studies using PUT for **CYE**. There was a decrease in lifetime from 0.96 ns to 0.28 ns for **CYE**; however, the radiative rate constant (k_r: 10^6 s^{-1}) was higher for the probe (83) than for the probe + PUT (36). A large non-radiative rate constant (k_{nr} = 10^6 s^{-1}) of 3534 after PUT addition is responsible for the low quantum yield. Detailed lifetime decay data for **CYE** and **CYA** are provided in Table S4 and Fig. S15.

The transformation of sharp, well-defined diffraction peaks into broader signals in the powder X-ray diffraction (PXRD) profiles indicates a significant loss of crystallinity upon exposure to amine vapors, which can also change the optical features of the materials (Fig. S16).[41] To gain a better understanding of various morphological forms of both samples after exposure to PUT and EDA vapors, scanning electron microscopy (SEM) images were captured (Fig. S17). The images clearly show the morphological differences before and after fuming with amine.

Photostability studies

The probes **CYE** and **CYA** showed spectral blue shifts of 84 nm and 49 nm when exposed to PUT and EDA vapors, respectively. Upon interaction with the diamines, **CYE** formed an amine adduct, whereas **CYA** formed the corresponding salt. Photostability studies were performed on the pristine probes (**CYE** and **CYA**) and their amine-treated forms (Fig. S18). The photostability of all four species was evaluated under continuous UV irradiation at their respective absorption λ_{max} for 1 h. All compounds exhibited excellent photostability before and after treatment with respective diamines, with an almost unchanged emission intensity upon irradiation (Fig. S18).

Theoretical investigation

The DFT-optimized molecular structure reveals a conformational twist in the molecule, with 1,2-dimethoxybenzene exhibiting a torsion angle of ~75–77° relative to the anthracene ring. Ground-state (S_0) optimization, optical absorption, and excited-state calculations were carried out using DFT and TD-DFT methods with the CAM-B3LYP functional and the 6-31G(d) basis set using Gaussian 09.[42] Toluene was used as a solvent to mimic the organic environment. The polarizable continuum model (PCM) was used to model the solvent.[43] A natural transition orbital (NTO) analysis was performed to find the nature of the excited state of emission (Fig. 7).[44] From the NTO analysis, we observed that fluorescence originates mostly from the transitions between the cyanoester orbitals, even in the monoamide and diamide adducts. Thus, their fluorescence energies are similar (0.979), and the calculated fluorescence wavelengths for cyanoester, cyano-monoamide adduct, and cyano-diamide adduct are 615.85 nm, 604.65 nm, and 609.37 nm, respectively (Table S5b). The emission of **CYE** is around 596 nm, which matches well with our calculated results (615.85 nm, Table S5b). A slight blue shift of the emission occurs in the presence of amide, which forms a cyanoamide adduct.

Detection of the freshness of Indian cottage cheese

To demonstrate their on-site application, we tested the sensitivity of both acid and ester probes using a real sample. The probe was drop-cast onto Whatman filter paper and placed in a sealed glass jar containing cottage cheese. The jar was sealed with a rubber septum, and an empty jar served as a control. The **CYE** probe showed quenching after 28 hours, while the **CYA** probe showed quenching after 6 hours. Interestingly, the **CYA** probe was more responsive to a mixture of amine vapors

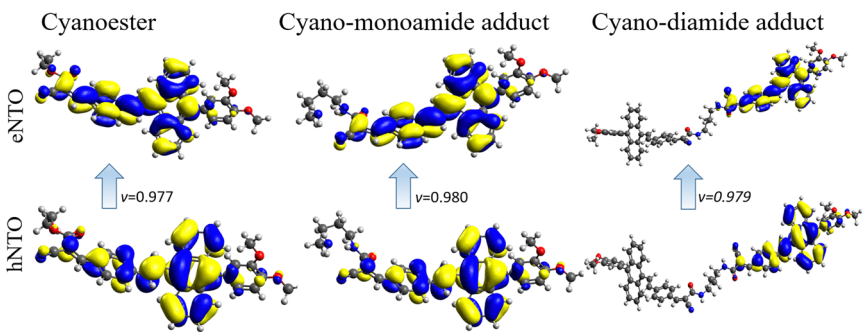

Fig. 7 Natural transition orbital (NTO) pairs for the S1 excited states. Hole and particle wave functions with the largest weight, ν, are placed below and above the arrows, respectively.

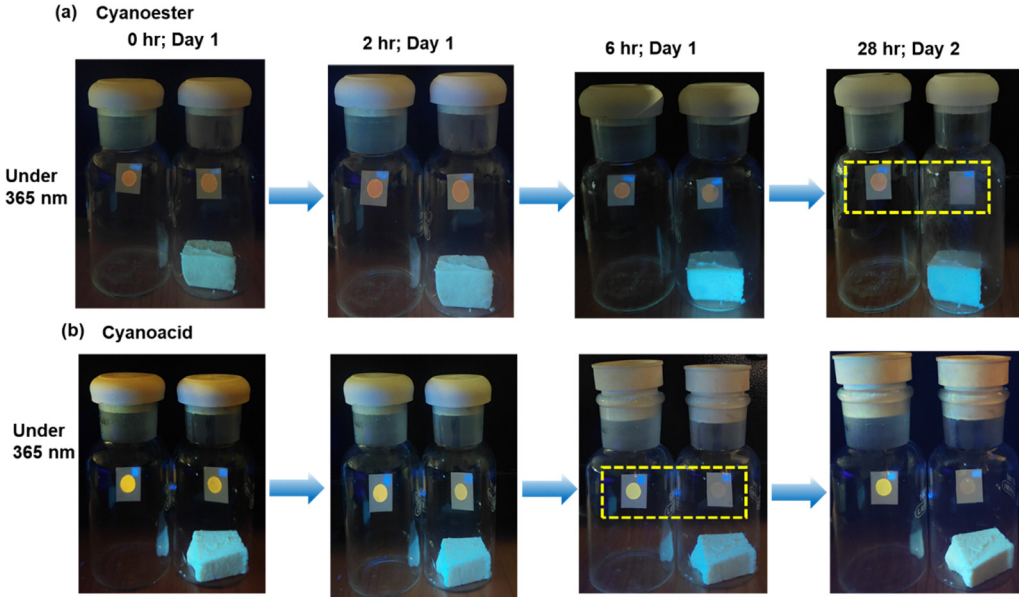

Fig. 8 Application of (a) **CYE** and (b) **CYA** in detecting the freshness of Indian cottage cheese.

produced by spoiled cottage cheese (Fig. 8). This sensing performance was validated by measuring the emission spectra, which showed a gradual reduction in intensity with time (Fig. S19).

Conclusion

This work describes a historically renowned reaction between a fluorophore, **CYE**, and diamines, which is utilized for the rapid detection of various amine and diamine vapors. Interestingly, the biogenic amine PUT, along with shorter-chain diamines, also undergoes stepwise reactions to produce mono- and diamides effectively. A sharp, rapid change in emission from red to green or yellow was visually detectable. The concentration-based changes in emission were also notable. Importantly, **CYE** is an AIEgen-based probe for detecting biogenic diamines *via* a 1,2-addition/elimination reaction. This observation was compared with the acid analogue, which displayed a color change only with EDA and Bu-NH_2, but not with any BAs. The detailed FT-IR, mass, and NMR analyses show a stepwise 1,2-addition/elimination reaction between **CYE** and diamine, whereas the acid analog **CYA** forms a salt with diamine. Notably, the practical utility of these fluorophores was illustrated by monitoring the freshness of Indian cottage cheese (paneer), where both probes displayed fluorescence quenching, while the acid analogs appeared to be a more sensitive platform.

Experimental

Materials and methods

All the required chemicals were purchased from various companies and used without purification. All the products were characterized by ^{1}H and ^{13}C NMR spectroscopy. NMR spectra were recorded on a Bruker 400 MHz instrument (400 MHz for ^{1}H NMR and 101 MHz for ^{13}C NMR). ^{1}H NMR experiments are reported in units of parts per million (ppm) and were measured relative to residual DMSO (2.50 ppm) in the deuterated solvent. ^{13}C NMR spectra are reported in ppm relative to deuterated DMSO (39.52 ppm), and all were obtained with ^{1}H decoupling. Coupling constants were reported in Hz. Reactions were monitored by thin-layer chromatography (TLC). Liquid chromatography–mass spectrometry (LC–MS) was performed by electron spray ionization (ESI) using a Q-TOF mass analyzer and reported as *m*/*z* (relative intensity). Melting points of the compounds were recorded on a KRUSS Optronic M3000 apparatus.

Steady-state absorption and fluorescence measurements

In the solution state, the electronic absorption spectra were recorded using a Shimadzu UV 3600 Plus. The fluorescence spectra were recorded using a quartz cuvette with a path length of 1 cm on a Hitachi spectrofluorometer (F7000, Japan). The solid-state emission spectra were recorded using a Fluorolog (Horiba). A stock solution of 0.001 M was prepared in DMAc. The final concentration of the probe was 10 μM.

Absolute quantum yield and lifetime decay measurement

The solid-state absolute quantum yield was measured using a calibrated integrating sphere method, with an accuracy of ±2%. Time-resolved fluorescence measurements were performed using a time-correlated single-photon counting (TCSPC) system (Horiba Deltaflex) with 440 nm and 510 nm lasers as the excitation source for all samples. Fluorescence decay data were fitted to ensure that the χ^2 value was close to 1, indicating a good fit. All experiments were performed at room temperature.

Powder X-ray diffraction (PXRD) and field-emission scanning electron microscopy (FE-SEM) study

PXRD measurements were performed using a Xenocs Nano-in Xider SW-L SAXS/WAXS 181 system equipped with a dual detector and a Cu K_α micro-focus source. Scans were conducted over a 5°–50° range at a scan rate of 2° per minute. The sample was evenly spread onto Kapton tape, and data were collected using transmission geometry. The FE-SEM images were recorded on solid samples dispersed in carbon tape using an FEI Apreo LoVac instrument.

Preparation of amine solutions

The solutions of amines were prepared in *N*,*N*-dimethylacetamide (DMAc). Initially, the absorption and emission spectra were recorded for **CYE** and **CYA**, followed by the addition of 20 μL of BAs from a 0.01 M stock solution.

Solid-state fuming

To induce solid-state changes, 10 mg of each compound (**CYE** and **CYA**) was placed in glass vials inside a sealed TLC chamber containing 1 mL of liquid amine. The chamber was left undisturbed for 12 hours, allowing amine vapors to fume the compounds uniformly. This fumed sample was used for ^{1}H NMR, FT-IR, PXRD, lifetime decay and absolute quantum yield measurements, solid-state UV-vis spectroscopy, and fluorescence spectroscopy.

Thin film study

10 mM solutions of **CYE** and **CYA** probes in dioxane were drop-cast onto glass coverslips. Once the solvent had evaporated and the slips were dry, they were attached to the inner wall of a 200 mL glass jar. Different amounts of amine were added to the jar, which was then sealed with a septum and wrapped with Teflon tape to prevent leakage. The color change of the probes was observed under a 365 nm UV lamp. After 20 minutes, the coverslips were removed and their fluorescence spectra were recorded. The concentration and limit of detection (LOD) of the probes with the amines were calculated in mg L^{-1}. Photographs of the coverslips were taken using a smartphone camera.

Synthetic procedures and characterization

Synthesis of (*E*)-4-(2-(10-(3,4-dimethoxyphenyl)anthracen-9-yl)vinyl)benzaldehyde (DAA). In a 50 mL round-bottomed flask, diethyl((10-(3,4-dimethoxyphenyl)anthracen-9-yl)methyl)phosphonate (0.10 g, 0.215 mmol) was dissolved in 10 mL of dry DMF under a nitrogen atmosphere at 25 °C followed by the addition of NaH dispersed in 60% paraffin oil (0.029 g, 1.29 mmol) in the reaction mixture at 0 °C and stirred for 10 min. Terephthaldehyde (0.072 g, 0.538 mmol) was added slowly to the reaction mixture. The reaction was stirred for 30 minutes, and the progress was monitored by TLC. The reaction mixture was quenched with water, extracted with ethyl acetate (3 × 30 mL), dried over anhydrous sodium sulfate, and concentrated under reduced pressure using a rotary evaporator. The compound **DAA** was purified by column chromatography (100–200 mesh silica gel) with petroleum ether to yield a yellow solid.

DAA. Yield 49% (0.047 g), M.P. 241–243 °C, IR (ν cm^{-1}, in KBr): 2921, 1694, 1604, 1224, 1126. ^{1}H NMR (400 MHz, $CDCl_3$) δ 10.01 (s, 1H), 8.31–8.29 (m, 2H), 8.10 (d, J = 16.5 Hz, 1H), 7.93–7.91 (m, 2H), 7.79–7.77 (m, 2H), 7.70–7.68 (m, 2H), 7.43–7.40 (m, 2H), 7.34–7.30 (m, 2H), 7.05–7.00 (m, 2H), 6.97–6.92 (m, 1H), 6.89–6.88 (m, 1H), 3.97 (s, 3H), 3.80 (s, 3H). ^{13}C NMR (101 MHz, $CDCl_3$) δ 191.7, 148.9, 148.5, 143.2, 137.5, 136.3, 135.7, 131.8, 131.2, 130.4, 130.3, 129.6, 129.3, 129.1, 129.0, 127.6, 127.0, 125.8, 125.5, 125.2, 123.5, 114.4, 111.1, 56.0, 55.9. HR-MS for $C_{31}H_{25}O_3$, calc. 445.1804, found 445.1788.

Synthesis of a diastereomeric mixture of ethyl 2-cyano-3-(4-((*E*)-2-(10-(3,4-dimethoxyphenyl)anthracen-9-yl)vinyl)phenyl)-acrylate and ethyl (*E*)-2-cyano-3-(4-((*E*)-2-(10-(3,4-dimethoxyphenyl)anthracen-9-yl)vinyl)phenyl)acrylate (CYE). In a 50 mL round-bottomed flask, (*E*)-4-(2-(10-(3,4-dimethoxyphenyl)anthracen-9-yl)vinyl)benzaldehyde (0.2 g, 0.45 mmol) and ethyl cyanoacetate (0.14 mL, 1.35 mmol) were dissolved in 20 mL of chloroform under a nitrogen atmosphere at room temperature. Then piperidine (0.08 mL, 0.9 mmol) was added, and the reaction mixture was heated to reflux for 12 hours at 60 °C. The reaction was monitored by TLC. The reaction mixture was quenched with water, extracted with dichloromethane (3 times, 30 mL each), dried over anhydrous sodium sulfate, and concentrated under reduced pressure using a rotary evaporator. The compound **CYE** was purified by column chromatography (100–200 mesh silica gel) using a 50% ethyl acetate–hexane mixture to yield an orange solid (diastereomeric ratio: 3 : 2, as determined by ^{1}H NMR).

CYE. Yield 64% (0.156 g), M.P. 225–227 °C, IR (ν cm^{-1}, in KBr): 2940, 2219, 1719, 1593, 1251. ^{1}H NMR (400 MHz, $CDCl_3$) δ 8.30–8.28 (m, 2H), 8.23–8.21 (m, 1H), 8.15–8.01 (m, 5H), 7.93–7.92 (m, 1H), 7.77–7.68 (m, 6H), 7.55–7.52 (m, 1H), 7.46–7.37 (m, 3H), 7.35–7.23 (m, 6H), 7.17–7.10 (m, 3H), 7.07–6.98 (m, 5H), 6.95–6.86 (m, 3H), 4.38–4.32 (m, 2H), 4.24 (q, J = 7.2 Hz, 2H), 3.98–3.94 (m, 6H), 3.87–3.86 (m, 2H), 3.80–3.78 (m, 4H), 1.38–1.37 (m, 1H), 1.36–1.35 (m, 1H), 1.34–1.33 (m, 1H), 1.27 (t, J = 7.2 Hz, 3H). ^{13}C NMR (101 MHz, $CDCl_3$) δ 162.7, 154.24, 148.9, 148.5, 142.1, 137.6, 136.1, 131.8, 131.7, 131.2, 130.9, 130.3, 129.3, 129.0, 127.7, 127.5, 127.2, 125.7, 125.5, 125.3, 125.2, 123.5, 115.8, 114.3, 111.1, 102.3, 62.7, 56.0, 55.9, 14.2. HR-MS for $C_{36}H_{29}NNaO_4$, calc. 562.1989, found 562.1990.

Synthesis of a diastereomeric mixture of 2-cyano-3-(4-((*E*)-2-(10-(3,4-dimethoxyphenyl)anthracen-9-yl)vinyl)phenyl)acrylic acid (CYA). In a 50 mL round-bottomed flask, (*E*)-4-(2-(10-(3,4-dimethoxyphenyl)anthracen-9-yl)vinyl)benzaldehyde (0.2 g, 0.45 mmol) and cyanoacetic acid (0.114, 1.35 mmol) were dissolved in 20 mL of chloroform under a nitrogen atmosphere at room temperature. Then piperidine (0.08 mL, 0.9 mmol) was added, and the reaction mixture was heated to reflux for 12 h at 60 °C. The completion of the reaction was monitored by TLC. The reaction mixture was quenched with water, extracted with dichloromethane (3 × 30 mL), dried over anhydrous sodium sulfate, and concentrated under reduced pressure using a rotary evaporator. The compound **CYA** was

purified by column chromatography (100–200 mesh silica gel) using a 60% ethyl acetate–hexane mixture to yield an orange solid (diastereomeric ratio: 1 : 1, as determined by ^{1}H NMR). Yield 67% (0.162 g), M.P. 219–221 °C, IR (ν cm^{-1}, in KBr): 3427, 2920, 2216, 1710, 1587. ^{1}H NMR (400 MHz, DMSO-d$_6$) δ 8.42–8.36 (m, 5H), 8.20–8.18 (m, 2H), 8.08–8.00 (m, 6H), 7.86–7.85 (m, 1H), 7.70–7.65 (m, 4H), 7.58–7.52 (m, 4H), 7.49–7.40 (m, 5H), 7.35–7.32 (m, 1H), 7.24–7.12 (m, 2H), 7.09–6.92 (m, 6H), 3.91 (m, 6H), 3.82–3.80 (m, 1H), 3.75–3.73 (m, 5H). ^{13}C NMR (101 MHz, DMSO-d$_6$) δ 163.7, 150.2, 149.2, 148.8, 140.6, 137.3, 136.8, 132.5, 130.9, 130.8, 130.2, 129.2, 128.2, 128.0, 127.8, 127.4, 126.3, 126.2, 126.1, 126.0, 123.7, 123.5, 118.6, 115.0, 114.9, 112.4, 56.1, 56.0. LC-MS for $C_{34}H_{24}NO_4$, calc. 510.1705, found 510.0000.

Author contributions

The manuscript was drafted by AJ and MC and later revised by all authors. All authors have given approval to the final version of the manuscript. AJ conceptualized and designed the project, synthesized all the probes, conducted the experiments, and contributed to data collection and analysis; SN and PKS performed computational calculations and data analysis. MC initiated and supervised the project, secured funding, and was actively involved in project planning, data interpretation, manuscript preparation, and revision.

Conflicts of interest

There are no conflicts to declare.

Data availability

The data supporting this article are included in the manuscript and supplementary information (SI). Supplementary information: characterization data and all the relevant spectra. See DOI: https://doi.org/10.1039/d6ma00194g.

Acknowledgements

We thank SERB [CRG/2022/001499] and LSRB [389/FSH&ABB/2021] for financial support. BITS-Pilani Hyderabad Campus X-ray diffraction and NMR facilities are acknowledged. Akshita thanks CSIR for her fellowship. The DST-FIST HR-MS facility SR/FST/CS-I/2020/158 and DSR-PURSE support are also acknowledged.

References

1 A. E. Crolais, C. Chen, J. Gao, N. D. Dolinski, Y. Xu, J. J. de Pablo, S. A. Snyder and S. J. Rowan, *J. Org. Chem.*, 2025, **90**, 4037–4045.
2 M. Kuhnert, H. Köster, R. Bartholomäus, A. Y. Park, A. Shahim, A. Heine, H. Steuber, G. Klebe and W. E. Diederich, *Angew. Chem., Int. Ed.*, 2015, **54**, 2849–2853.
3 G. L. Jackson, J. M. Dennis, N. D. Dolinski, M. van der Naald, H. Kim, C. Eom, S. J. Rowan and H. M. Jaeger, *Macromolecules*, 2022, **55**, 6453–6461.
4 H. Lee, Y. Kim, H. Aziz, D. M. Kang, J. Lee, S. Lee, S. Jung, S. Hyeon, H. Choo, G. Nam, Y. K. Kim, S. Lim and S. J. Min, *Bioorg. Med. Chem.*, 2023, **95**, 117513.
5 T. Hill, L. R. Odell, J. K. Edwards, M. E. Graham, A. B. McGeachie, J. Rusak, A. Quan, R. Abagyan, J. L. Scott, P. J. Robinson and A. McCluskey, *J. Med. Chem.*, 2005, **48**, 7781–7788.
6 T. A. Hill, J. A. Sakoff, P. J. Robinson and A. McCluskey, *Aust. J. Chem.*, 2005, **58**, 94–103.
7 T. Wang, L. Shen, H. Wang and N. Zhang, *J. Mol. Struct.*, 2021, **1231**, 129671.
8 S. Suganya, E. Ravindran, M. K. Mahato and E. Prasad, *Sens. Actuators, B*, 2019, **291**, 426–432.
9 A. Lorente, L. Vaquerizo, A. Martín and P. Gómez-Sal, *Heterocycles*, 1995, **41**, 71–86.
10 B. Prusti, S. Tripathi, A. Jain and M. Chakravarty, *ACS Appl. Mater. Interfaces*, 2023, **15**, 16492–16504.
11 M. Chakraborty, P. Sivasakthi, P. K. Samanta and M. Chakravarty, *J. Mater. Chem. B*, 2024, **12**, 2746–2760.
12 A. Jain, P. Sivasakthi, P. K. Samanta and M. Chakravarty, *J. Org. Chem.*, 2024, **89**, 4384–4394.
13 (*a*) S. Singh, K. Mandal and M. Chakravarty, *Chem. Commun.*, 2025, **61**, 728–731; (*b*) S. Tripathi, B. Prusti and M. Chakravarty, *Commun. Chem.*, 2025, **8**, 81.
14 D. Doeun, M. Davaatseren and M. S. Chung, *Food Sci. Biotechnol.*, 2017, **26**, 1463–1474.
15 P. Herbert, M. J. Cabrita, N. Ratola, O. Laureano and A. Alves, *J. Food Eng.*, 2005, **66**, 315–322.
16 M. H. Silla Santos, *Int. J. Food Microbiol.*, 1996, **29**, 213–231.
17 Y. Guo, Y. P. Yang, Q. Peng and Y. Han, *Int. J. Food Sci. Technol.*, 2015, **50**, 1523–1532.
18 A. Halász, A. Baráth, L. Simon-Sarkadi and W. Holzapfel, *Trends Food Sci. Technol.*, 1994, **5**, 42–49.
19 A. Onal, *Food Chem.*, 2007, **103**, 1475–1486.
20 G. Munzi, S. Failla and S. Di Bella, *Analyst*, 2021, **146**, 2144–2151.
21 N. Verma, V. Hooda, A. Gahlaut, A. Gothwal and V. Hooda, *Crit. Rev. Biotechnol.*, 2020, **40**, 1–14.
22 M. Papageorgiou, D. Lambropoulou, C. Morrison, E. Kłodzinska, J. Namieśnik and J. Płotka-Wasylka, *TrAC, Trends Anal. Chem.*, 2018, **98**, 128–142.
23 (*a*) R. L. Self, W.-H. Wu and H. S. Marks, *J. Agric. Food Chem.*, 2011, **59**, 5906–5913; (*b*) Z. Song, M. Cai, Y. Zhao, M. Jin and S. Deng, *Anal. Methods*, 2015, **7**, 7436–7442.
24 L. Zeng, X. Xiao, H. Ye, D. Ma and J. Zhou, *Food Chem.*, 2022, **394**, 133489.
25 R. Roy, A. Pramanik, T. Dutta, V. Sharma, Kovida and A. L. Koner, *Mater. Chem. Front.*, 2022, **6**, 3489–3503.
26 B. Zhu, L. Jiang, T. Chen, G. Bao, L. Zeng, X. Hu and H. Yuan, *Dyes Pigm.*, 2021, **186**, 108963.
27 S. Sentellas, Ó. Núñez and J. Saurina, *J. Agric. Food Chem.*, 2016, **64**, 7667–7678.
28 M. Venkateswarulu, P. Gaur and R. R. Koner, *Sens. Actuators, B*, 2015, **210**, 144–148.

29 H. Ahangari, S. Kurbanoglu, A. Ehsani and B. Uslu, *Trends Food Sci. Technol.*, 2021, **112**, 75–87.
30 Y. Hu, T. Han, N. Yan, J. Liu, X. Liu, W.-X. Wang, J. W. Y. Lam and B. Z. Tang, *Adv. Funct. Mater.*, 2019, **29**, 1902240.
31 L. Wang, X. Ran, H. Tang and D. Cao, *Dyes Pigm.*, 2021, **194**, 109634.
32 A. R. Longstreet, M. Jo, R. R. Chandler, K. Hanson, N. Zhan, J. J. Hrudka, H. Mattoussi, M. Shatruk and D. T. McQuade, *J. Am. Chem. Soc.*, 2014, **136**, 15493–15496.
33 D. R. Turner, A. J. Edwards and R. O. Piltz, *CrystEngComm*, 2012, **14**, 6447–6464.
34 S. Tripathi and M. Chakravarty, *Chem. – Eur. J.*, 2025, **31**, e202403300.
35 M. Z. Baig, D. Majhi, R. P. Tulichala, M. Sarkar and M. Chakravarty, *J. Mater. Chem. C*, 2017, **5**, 2380–2387.
36 N. J. Hestand and F. C. Spano, *Chem. Rev.*, 2018, **118**, 7069–7163.
37 K. Saeki, K. Ikari, H. Yokoi, S.-I. Ohira, H. Okochi and K. Toda, *ACS Earth Space Chem.*, 2022, **6**, 421–430.
38 Ethylenediamine CAS#: 107-15-3, ChemicalBook, available at: https://m.chemicalbook.com/ProductChemicalPropertiesCB2127811_EN.htm.
39 Hexamethylenediamine CAS#: 124-09-4, ChemicalBook, available at: https://m.chemicalbook.com/ProductChemicalPropertiesCB7204696_EN.htm.
40 (*a*) R. M. Silverstein, F. X. Webster and D. J. Kiemle, *Spectrometric Identification of Organic Compounds*, 7th edn, John Wiley & Sons, Hoboken, NJ, 2005, pp. 102–103; (*b*) B. C. Smith, *Spectroscopy*, 2018, **33**, 14–20.
41 B. Prusti, P. K. Samanta, N. J. English and M. Chakravarty, *Chem. Commun.*, 2021, **57**, 12321–12324.
42 M. J. Frisch, *et al.*, *Gaussian 09, Revision A.02*, Gaussian, Inc., Wallingford CT, 2016.
43 G. Scalmani and M. J. Frisch, *J. Chem. Phys.*, 2010, **132**, 144110.
44 R. L. Martin, *J. Chem. Phys.*, 2003, **118**, 4775–4777.